A novel external reflecting raceway pond design for improved biomass productivity

Jack Hoeniges [a,b], William Welch [a], Jeremy Pruvost [b], Laurent Pilon [a,*]

[a] *Mechanical and Aerospace Engineering Department, Henry Samueli School of Engineering and Applied Science, University of California, 420 Westwood Plaza, Los Angeles, CA 90095, USA*
[b] *Université de Nantes, Oniris, CNRS, GEPEA, UMR 6144, F-44600 Saint-Nazaire, France*

ARTICLE INFO

ABSTRACT

Outdoor raceway ponds for microalgae cultivation suffer from low biomass productivity due in part to the low photosynthetic photon flux received by the microalgae culture in the mornings and evenings and during the winter months at middle and high latitudes. This study explores the use of external mirrors to reflect additional sunlight onto the culture and increase the incident solar flux at critical times of the day and year. Four designs cultivating *Chlorella vulgaris* were considered: a raceway pond without mirrors (Configuration A), a pond oriented along the north/south axis with dual east/west mirrors (Configuration B), a pond oriented along the east/west axis with a single north mirror (Configuration C), and a solar tracking rotating pond with a single mirror (Configuration D). The biomass productivity was predicted by coupling the simulated radiative field within the culture to a microalgae growth kinetics model accounting for photolimitation and biomass loss due to respiration. Two different locations were considered, namely Los Angeles, CA, USA and Saint-Nazaire, France. The use of mirrors was predicted to increase the daily culture-area-based and volumetric biomass productivity at both locations and all months of the year. Configuration D yielded the highest biomass productivity year-round. Configuration B had a higher biomass productivity than Configuration C in the summer months and vice versa in the winter months. Overall, Configuration C was considered to be the simplest and most cost-effective method to increase raceway productivity. Indeed, this configuration improved the raceway pond volumetric and culture-area-based biomass productivity by as much as 73% in the winter months compared to Configuration A. Additionally, the impact of operational parameters (initial biomass concentration and culture depth) and design parameters (pond length-to-width ratio and mirror height) were assessed to provide practical recommendations for maximizing biomass productivity.

1. Introduction

Microalgae have garnered interest as a source of biomass for carbon-neutral biofuels [1], as a fast-growing crop for human and animal feed [2], and as a valuable ingredient in food supplements, nutraceuticals, and cosmetics [3]. Currently, microalgae are produced in large-scale outdoor raceway ponds consisting of a culture, at least 15 cm deep, and oriented along the north/south axis [4,5]. For raceway ponds in outdoor conditions, large solar incidence angles occur in the mornings and evenings and during the winter months when the solar elevation angle may be small depending on the latitude where the raceway pond is operated. As a result, the incident spectral solar radiative flux $q_{in,\lambda}''(t)$ decreases compared to situations when sunlight is nearly normally

incident on the culture according to [6]

$$q_{in,\lambda}''(t) = G_{S,\lambda}(t)cos\theta_z(t) \tag{1}$$

where $G_{S,\lambda}$ is the time-dependent spectral collimated solar irradiation and θ_z is the solar zenith angle for a given time of day t, defined with respect to the outward pointing normal vector of the microalgae culture surface. Furthermore, sunlight delivered at oblique angles does not penetrate as deeply into the microalgae culture compared to normally incident light [7,8]. Thus, non-normal incidence can increase dark zones in the culture where there is not enough light to drive photosynthesis. This phenomenon, combined with the decrease in solar irradiation in the mornings and evenings, negatively impacts microalgae growth by reducing the amount of light available to the suspended cells.
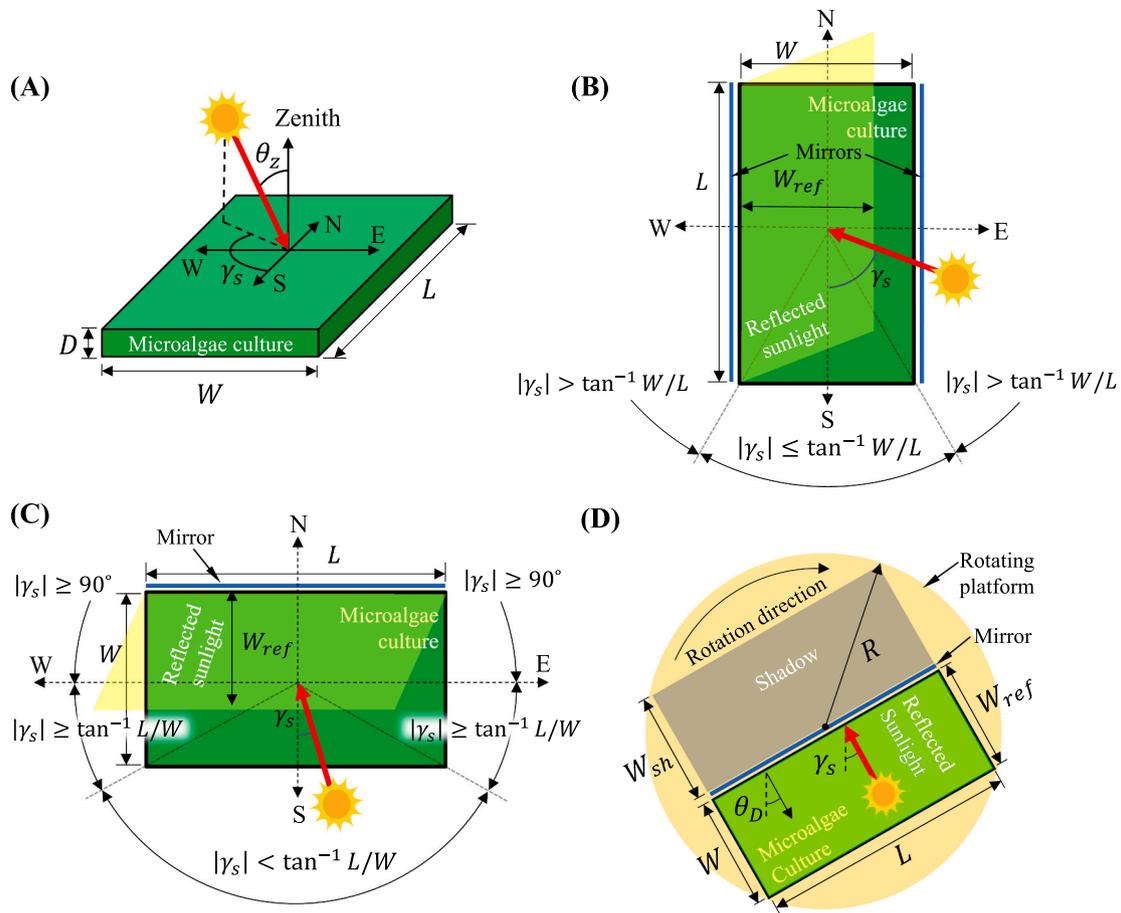
Fig. 1. Top view (not to scale) of (A) Configuration A: a $L \times W$ raceway pond without mirrors, (B) Configuration B: a raceway pond featuring dual vertical mirrors on its east and west sides, (C) Configuration C: a raceway pond featuring a single vertical mirror on its north side, and (D) Configuration D: a raceway pond and mirror on a rotating platform tracking the sun throughout the day.

The aim of this study is to explore the use of mirrors to increase the biomass productivity of raceway ponds by increasing the solar radiative flux delivered to the microalgae culture at critical times of the day and year. The daily biomass productivity of a raceway pond with various configurations of vertical mirrors was predicted throughout the year using experimentally-validated models coupling light transfer and growth kinetics. The performance of each configuration was assessed in terms of areal and volumetric productivities and compared to the same raceway pond but without mirrors. The impact of operating parameters, such as initial biomass concentration and culture depth, and of design parameters including mirror height, pond length-to-width ratio, and cultivation location, were assessed.

2. Methods

2.1. Problem statement

Let us consider an outdoor rectangular raceway pond of width $W = 1$ m and length $L = 2$ m located in either Los Angeles, CA, USA (34.07° N, 118.44° W) or Saint-Nazaire, France (47.25° N, 2.26° W) growing a culture of *Chlorella vulgaris* of depth D equal to 0.1 m, 0.2 m, or 0.3 m. These locations were chosen due to their difference in latitude in the northern hemisphere. The pond was exposed to direct, collimated solar radiation $G_{S,\lambda}$ (in $\mu mol_{h\nu} m^{-2} s^{-1}$) from sunrise to sunset on September 21st as depicted in Fig. 1A. September 21st was considered representative of an average day as there are approximately 12 h of sunlight in Los Angeles, CA on this day. The daily biomass productivity was also simulated for the 21st day of each month of the year. The raceway ponds

were considered to be operated in a semi-continuous mode where harvesting took place when the maximum daily biomass concentration X_{max} (in kg m^{-3}) was attained, i.e., at time $t(X = X_{max})$. The solar position for a given time and day was described by the solar zenith angle θ_z and the solar azimuth angle γ_s defined with respect to the due south direction, as illustrated in Fig. 1A. Here, $\gamma_s = -90°$ corresponded to due east and $\gamma_s = 90°$ corresponded to due west.

2.1.1. Novel pond design and control

Four different designs were investigated to explore the use of vertical external mirror(s) as a simple way to reflect additional direct sunlight onto the culture and improve the microalgae growth rate, particularly when the sun was low on the horizon, i.e., when the solar zenith angle θ_z was large. Configuration A consisted of a standard raceway pond without mirrors oriented lengthwise along the north/south axis (Fig. 1A). Configuration B consisted of the same raceway pond as in Configuration A but featuring two vertical mirrors on its east and west sides of time-dependent height $H_{B,E}(t)$ and $H_{B,W}(t)$, respectively (Fig. 1B). Here, the eastern mirror was lowered and the western mirror was raised in the morning and vice versa in the afternoon. Similarly, Configuration C consisted of the same raceway pond as in Configuration A but oriented lengthwise along the east/west axis and featuring a single vertical mirror on its north side with time-dependent height $H_C(t)$ (Fig. 1C). Finally, Configuration D consisted of the same raceway pond as in Configuration A but on a circular rotating platform of radius R tracking the movement of the sun throughout the day and featuring a single vertical mirror of time-dependent height $H_D(t)$ (Fig. 1D). Here, the platform rotation angle θ_D was defined as the angle between the due

(a)

(b)
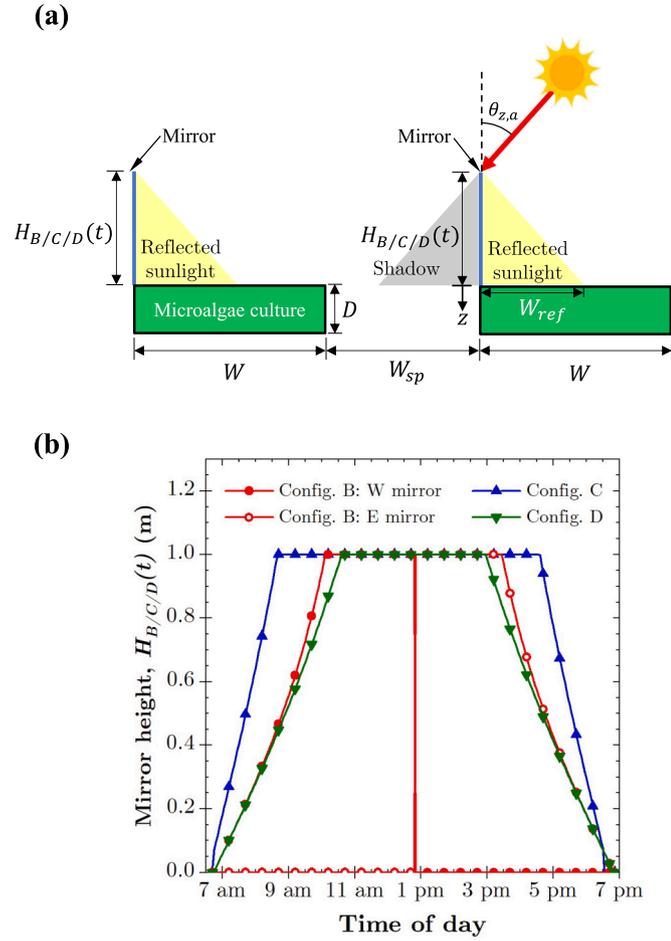
Fig. 2. (a) A side view (not to scale) of Configurations B–D illustrating the reflection width W_{ref}, pond spacing width W_{sp}, and the apparent solar zenith angle $\theta_{z,a}$. (b) Mirror height $H_{B/C/D}(t)$ given by Eqs. (2)–(4) as a function of time of day on September 21st in Los Angeles, CA for maximum allowed mirror height $H^* = 1$ m.

south direction and the outward pointing normal vector of the mirror. As with the solar azimuth angle γ_s, a rotation angle of $\theta_D = -90°$ corresponded to a due east-facing mirror position and $\theta_D = 90°$ corresponded to a due west-facing mirror position. Configuration D was considered to assess the maximum productivity achievable with the use of mirrors in a manner similar to Pruvost et al. [9] who considered the ideal case of a solar tracking photobioreactor to assess the maximum theoretical productivity of a solar photobioreactor.

The time-dependent mirror height $H_{B/C/D}(t)$ for Configurations B–D was controlled to maximize the culture surface area S_{ref} subjected to reflected light while minimizing mirror height to avoid shading between adjacent raceway ponds. When the magnitude of the solar azimuth angle $|\gamma_s| > \tan^{-1}(W/L)$ for Configuration B and $|\gamma_s| > \tan^{-1}(L/W)$ for Configuration C (see Fig. 1B and 1C) the reflected area was maximized by controlling the mirror height such that the reflected width W_{ref} was equal to the pond width, i.e., $W_{ref} = W$. However, when $|\gamma_s| > \tan^{-1}(W/L)$ for Configuration B and $|\gamma_s| > \tan^{-1}(L/W)$ for Configuration C, the reflected area was maximized for a reflected width $W_{ref} = L \tan|\gamma_s|$ and $W_{ref} = L/\tan|\gamma_s|$ for Configurations B and C, respectively. Then, the reflected width W_{ref} never exceeded the pond width W and shading between adjacent ponds was avoided for pond spacing width $W_{sp} = W$ for Configurations B and C and $W_{sp} = R = W\sqrt{2}$ for Configuration D. Fig. 2a depicts a schematic of the side view of Configurations B–D illustrating the spacing width W_{sp}. For each configuration, the mirror height $H_{B/C/D}(t)$ which gave the desired reflected width W_{ref} was calculated based on

the apparent solar zenith angle $\theta_{z,a}$, defined as the angle between the vertical axis and the incoming solar radiation as observed from a side view of a given configuration (see Fig. 2a). The apparent solar zenith angle $\theta_{z,a}$ was given by $\theta_{z,a} = \tan^{-1}(\tan\theta_z \sin|\gamma_s|)$ for Configuration B and by $\theta_{z,a} = \tan^{-1}(\tan\theta_z \cos|\gamma_s|)$ for Configuration C. For Configuration D, the platform supporting the pond was rotated such that the mirror was always facing the sun and the rotation angle θ_D was equal to the solar azimuth angle γ_s. Thus, the actual and apparent solar zenith angles were equal, i.e., $\theta_z = \theta_{z,a}$. Then, the mirror height $H_{B/C/D}$ for each configuration was given by

$$H_B(t) = \begin{cases} W/\tan\theta_{z,a}, & |\gamma_s| > \tan^{-1}(W/L) \\ L\tan|\gamma_s|/\tan\theta_{z,a}, & |\gamma_s| \le \tan^{-1}(W/L) \end{cases} \quad (2)$$

$$H_C(t) = \begin{cases} 0, & |\gamma_s| > 90° \\ L/\tan|\gamma_s|\tan\theta_{z,a}, & 90° > |\gamma_s| \ge \tan^{-1}(L/W) \\ W/\tan\theta_{z,a}, & |\gamma_s| < \tan^{-1}(L/W) \end{cases} \quad (3)$$

$$H_D(t) = W/\tan\theta_{z,a}. \quad (4)$$

To avoid unreasonably large values of mirror height when $\theta_{z,a}$ was small, a maximum allowed height of $H^* = 1$ m was imposed. Then, the mirror height for a given time t was the minimum value between H^* and the mirror height for a given configuration from Eqs. (2)–(4). Note that, for Configuration B, the west mirror height $H_{B,W}(t)$ was given by Eq. (2) while the east mirror was lowered in the morning when the solar azimuth angle was negative, i.e., $\gamma_z < 0$. Similarly, the east mirror height $H_{B,E}(t)$ was given by Eq. (2) while the west mirror was lowered in the afternoon when the solar azimuth angle was positive, i.e., $\gamma_s > 0$. Note that the mirror height $H_C(t)$ was equal to zero for Configuration C when the sun was positioned behind the mirror, i.e., $|\gamma_s| > 90°$. Fig. 2b plots the resulting mirror heights $H_{B/C/D}(t)$ as a function of time for Configurations B–D on September 21st according to Eqs. (2)–(4) with an imposed maximum mirror height of $H^* = 1$ m.

2.2. Assumptions

Light transfer and microalgae growth were modeled based on the following assumptions: (1) all mirrors were considered to be specularly-reflecting with 100% reflectivity over the photosynthetically active radiation (PAR) region from 400 to 750 nm. (2) The raceway pond was operated in the light-limited regime such that growth was only a function of the local rate of photon absorption (LRPA) within the culture. (3) Light transfer within the culture was considered to be one-dimensional along the z-axis and shading from the walls of the raceway pond was negligible, as demonstrated in Ref. [10]. (4) Diffuse solar radiation was neglected. (5) The culture was well-mixed with uniform biomass concentration. (6) The liquid medium was non-scattering and non-absorbing over the PAR region. (7) The radiative properties and kinetic growth parameters of *Chlorella vulgaris* were constant throughout the day. (8) The culture temperature was kept constant throughout the day. (9) The bottom of the raceway ponds were perfectly absorbing.

2.3. Reflected sunlight

The culture surface area subjected to reflected sunlight S_{ref} for a given configuration and solar position was calculated as the difference between the total surface area of light reflected by the mirror and the area of reflected light that fell outside of the culture surface (see Fig. 1B and 1C) according to

$$S_{ref}(t) = \begin{cases} W_{ref}(t)L - \frac{1}{2}W_{ref}(t)^2/|\tan\gamma_s(t)| & \text{for Configuration B} \\ W_{ref}(t)L - \frac{1}{2}W_{ref}(t)^2\tan\gamma_s(t) & \text{for Configuration C} \\ W_{ref}(t)L & \text{for Configuration D}. \end{cases} \quad (5)$$

The amount of additional light reflected onto the culture for each pond configuration can be assessed by considering the ratio S_{ref}/S_C of the culture surface area subjected to reflected sunlight S_{ref} to the total culture surface area $S_C = WL$. The ratio of S_{ref}/S_C ranged from zero, when none of the culture surface was exposed to reflected light, to 1.0 when the entire culture surface area was exposed to reflected light. Then, the incident mean spectral radiative flux $\overline{q}''_{in,\lambda}$ (in $\mu mol_{h\nu} m^{-2} s^{-1}$) averaged over the culture surface area at a given time t was given by

$$\overline{q}''_{in,\lambda}(t) = \tau(\theta_z(t)) G_{S,\lambda}(t) cos\theta_z(t) \left(1 + \frac{S_{ref}(t)}{S_C}\right) \tag{6}$$

where $\tau(\theta_z(t))$ is the transmittance of the air/microalgae culture interface predicted by Fresnel's equations for an incidence angle equal to the solar zenith angle θ_z [6]. Note that since the mirror was perfectly vertical, the angle of incidence of reflected light was equal to that of light directly incident on the culture surface. The resulting incident mean photosynthetic photon flux $\overline{q}''_{in,PAR}(t)$ was obtained by integrating $\overline{q}''_{in,\lambda}(t)$ over the PAR region, i.e.,

$$\overline{q}''_{in,PAR}(t) = \int_{PAR} \overline{q}''_{in,\lambda}(t) d\lambda. \tag{7}$$

2.4. Light transfer in microalgae culture

The two-flux approximation was used as an analytical solution to the one-dimensional radiative transfer equation governing light transfer in the microalgae culture. This method has been validated and used extensively in previous studies [7,10–14]. The radiation transmitted through the air/microalgae culture interface was refracted at the interface at an angle $\theta_m = \sin^{-1}(n_a/n_m \sin \theta_z)$ where $n_a = 1.0$ and $n_m = 1.33$ are the refractive indices of the air and culture medium, respectively. Then, for a raceway pond with a perfectly absorbing bottom wall and exposed to the mean incident spectral radiative flux $\overline{q}''_{in,\lambda}(t)$, the local spectral fluence rate $G_\lambda(z,t)$ at a given culture depth z (see Fig. 2a) was given by

$$\frac{G_\lambda(z,t)}{\overline{q}''_{in,\lambda}(t)} = \frac{2}{cos\theta_m} \frac{(1+\alpha_\lambda)e^{\delta_\lambda(D-z)} - (1-\alpha_\lambda)e^{-\delta_\lambda(D-z)}}{(1+\alpha_\lambda)^2 e^{\delta_\lambda D} - (1-\alpha_\lambda)^2 e^{-\delta_\lambda D}} \tag{8}$$

where the parameters α_λ and δ_λ were expressed as [13]

$$\alpha_\lambda = \sqrt{\frac{\overline{A}_{abs,\lambda}}{\overline{A}_{abs,\lambda} + 2b_\lambda \overline{S}_{sca,\lambda}}} \text{ and } \delta_\lambda = \frac{\alpha_\lambda X(t)}{cos\theta_m} \left(\overline{A}_{abs,\lambda} + 2b_\lambda \overline{S}_{sca,\lambda}\right). \tag{9}$$

Here, $X(t)$ is the biomass concentration (in kg m^{-3}) at time t while the spectral average mass absorption $\overline{A}_{abs,\lambda}$ and scattering $\overline{S}_{sca,\lambda}$ cross-sections (in m^{2}kg^{-1}) and the backward scattering ratio b_λ of *Chlorella vulgaris* were obtained from experimental measurements, reported in Ref. [8] and shown Fig. S1 of the Supplementary Materials. Finally, the local rate of photon absorption (LRPA) by the microalgae cells, denoted by $\mathscr{A}(z,t)$ (in $\mu mol_{h\nu}$ kg^{-1} s^{-1}), was defined as [8]

$$\mathscr{A}(z,t) = \int_{PAR} \overline{A}_{abs,\lambda} G_\lambda(z,t) d\lambda. \tag{10}$$

2.5. Microalgae growth kinetics

The time rate of change of the biomass concentration $X(t)$ in a microalgae batch culture can be expressed as [15]

$$\frac{dX}{dt} = \overline{r}_X(t) = \overline{\mu}(t)X(t) \tag{11}$$

where $\overline{r}_X(t)$ is the average volumetric growth rate (in kg m^{-3} s^{-1}) and $\overline{\mu}(t)$ is the volume-averaged specific growth rate (in s^{-1}). The growth kinetics model and corresponding parameters reported in Refs. [8,16]

Table 1
Growth kinetics parameters for *Chlorella vulgaris* [8].

Parameter	Value	Units
ρ_M	0.8	–
J_{NADH_2}	2.8×10^{-3}	$mol_{NADH_2} kg_X^{-1} s^{-1}$
ν_{O_2-X}	1.13	–
$\overline{\phi}'_{O_2}$	1.1×10^{-7}	$mol_{O_2} \mu mol_{h\nu}^{-1}$
M_X	0.024	$kg_X mol_C^{-1}$
$\nu_{NADH_2-O_2}$	2	–
K	40,000	$\mu mol_{h\nu} kg^{-1} s^{-1}$
K_r	556.5	$\mu mol_{h\nu} kg^{-1} s^{-1}$
$\mathscr{A}_c$	2800	$\mu mol_{h\nu} kg^{-1} s^{-1}$

for *C. vulgaris* are given in Table 1 and were used to predict the specific growth rate $\overline{\mu}(t)$ of the microalgae culture as a function of time. This model accounted for light limitation and cell respiration activity [16].

First, the volume-averaged specific rate of oxygen production or consumption $\overline{J}_{O_2}(t)$ (in $mol_{O_2} kg_X^{-1} s^{-1}$) as a function of the LRPA $\mathscr{A}(z,t)$ was calculated according to [8]

$$\overline{J}_{O_2}(t) = \frac{1}{D} \int_0^D \left[\rho_M \frac{K}{K + \mathscr{A}(z,t)} \overline{\phi}'_{O_2} \mathscr{A}(z,t) - \frac{J_{NADH_2}}{\nu_{NADH_2-O_2}} \frac{K_r}{K_r + \mathscr{A}(z,t)}\right] dz. \tag{12}$$

Here, ρ_M is the maximum energy yield for photon conversion, $\overline{\phi}'_{O_2}$ (in $mol_{O_2} \mu mol_{h\nu}^{-1}$) is the molar quantum yield of O_2 for the Z-scheme of photosynthesis, K (in $\mu mol_{h\nu}$ kg^{-1} s^{-1}) is the half-saturation constant for photosynthesis, J_{NADH2} (in $mol_{NADH2} kg_X^{-1} s^{-1}$) is the specific rate of cofactor regeneration on the respiratory chain related to the oxygen consumption by the stoichiometric coefficient of cofactor regeneration on the respiratory chain $\nu_{NADH2-O2}$, and K_r (in $\mu mol_{h\nu}$ kg^{-1} s^{-1}) is a saturation constant describing the inhibition of respiration in light.

Then, the stoichiometric relationship between the production of oxygen and the production of biomass was used to predict the volume-averaged growth rate $\overline{\mu}(t)$ (in s^{-1}) as a function of $\overline{J}_{O_2}(t)$ according to [8]

$$\overline{\mu}(t) = \frac{\overline{r}_X(t)}{X(t)} = \frac{\overline{J}_{O_2}(t)M_X}{\nu_{O_2-X}} \tag{13}$$

where M_X (in $kg_X mol_C^{-1}$) is the C-molar mass in the biomass given by CH_pO_n and ν_{O2-X} is the stoichiometric coefficient of the oxygen production.

2.6. Biomass productivity

The daily volumetric P_V, culture-area-based $P_{A,C}$, and land-area-based $P_{A,L}$ biomass productivities were considered as metrics to compare the performance of all four raceway pond configurations. The daily volumetric biomass productivity P_V (in kg m^{-3} day^{-1}) was defined as

$$P_V = \frac{(X_{max} - X_0)}{\Delta t} \tag{14}$$

where X_{max} is the maximum biomass concentration reached on a given day, X_0 is the initial biomass concentration, and the time increment Δt is equal to one day. Similarly, the daily culture-area-based biomass productivity $P_{A,C}$ (in kg m^{-2} day^{-1}) was defined as

$$P_{A,C} = \frac{(X_{max} - X_0)V}{S_C \Delta t} = P_V D \tag{15}$$

where S_C is the culture surface area. In addition, the daily land-area-based biomass productivity $P_{A,L}$ (in kg m^{-2} day^{-1}) was defined as

$$P_{A,L} = \frac{(X_{max} - X_0)V}{S_L \Delta t} \tag{16}$$
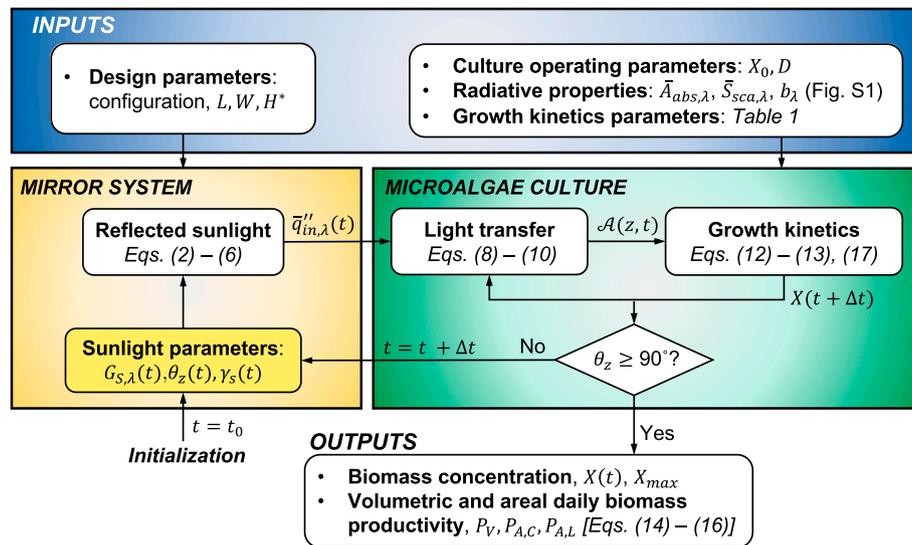
Fig. 3. Block diagram illustrating the computational procedure used for predicting the temporal evolution of biomass concentration $X(t)$ and the daily biomass productivities for raceway Configurations A–D.

where S_L is the land area required to accommodate both the raceway ponds and the spacing between adjacent ponds. The land area S_L required for a single pond was $S_L = 2S_C = 4\,m^2$ for Configurations B and C with pond width W and spacing width W_{sp} equal to 1 m. A circular land area $S_L = \pi R^2 = \pi(W^2 + L^2/4) = 6.28\,m^2$ was required for Configuration D.

The volumetric P_V, culture-area-based $P_{A,C}$, and land-area-based $P_{A,L}$ productivities were considered as they are related to the different costs associated with producing a kilogram of biomass. The volumetric productivity P_V can be used to assess the biomass output relative to the operating costs that depend on the culture volume such as the energy required for water circulation and thermal regulation as well as downstream processing costs such as dewatering [17]. The daily culture-area-based $P_{A,C}$ and land-area-based $P_{A,L}$ productivities can be used to assess the biomass output relative to operating and capital costs that scale with the culture area (e.g., evaporation losses, pond liners) and land area (e. g., land cost), respectively [18]. The land-area-based productivity $P_{A,L}$ can also be used to estimate the size of the facility required for a desired yield of biomass.

2.7. Boundary and initial conditions

The incident spectral solar irradiance $G_{S,\lambda}(t)$ was determined using the Simple Model of the Atmospheric Radiative Transfer of Sunshine (SMARTS) for either Los Angeles, CA or Saint-Nazaire, France on the 21st day of each month [19]. The initial biomass concentration X_0 was varied between (i) 0.03 and 0.30 kg m^{-3} for culture depth $D = 0.3$ m, (ii) 0.03 and 0.45 kg m^{-3} for $D = 0.2$ m, and (iii) 0.03 and 0.70 kg m^{-3} for $D = 0.1$ m. These ranges of culture depth and biomass concentration were found to yield positive biomass productivity on September 21st.

2.8. Method of solution

Fig. 3 shows a block diagram describing the process for predicting the biomass concentration $X(t)$ as a function of time for Configurations A–D. First, the solar conditions at sunrise, i.e., $t = t_0$, were used to calculate the mean incident spectral radiative flux $\bar{q}''_{in,\lambda}$ [Eqs. (2)–(6)] for a given configuration, pond length L, width W, and maximum allowed mirror height H^*. Then, the two-flux model was applied to predict the LRPA $\mathcal{A}(z,t)$ within the culture [Eqs. (8)–(10)] for a given initial biomass concentration X_0 and culture depth D and using the radiative properties of *Chlorella vulgaris* [8]. Next, the growth kinetics model for
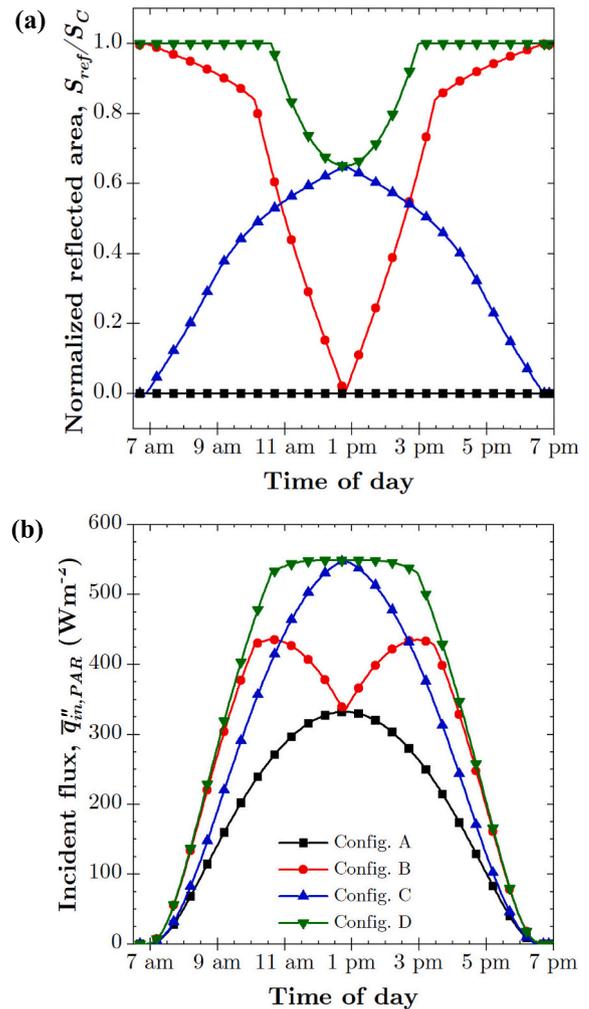
Fig. 4. (a) Fraction S_{ref}/S_C of the total culture surface area $S_C = WL$ subjected to reflected sunlight and (b) incident photosynthetic photon flux $\bar{q}''_{in,PAR}$ averaged over the culture surface area as a function of time on September 21st for Configurations A–D in Los Angeles, CA.

(a)

(b)
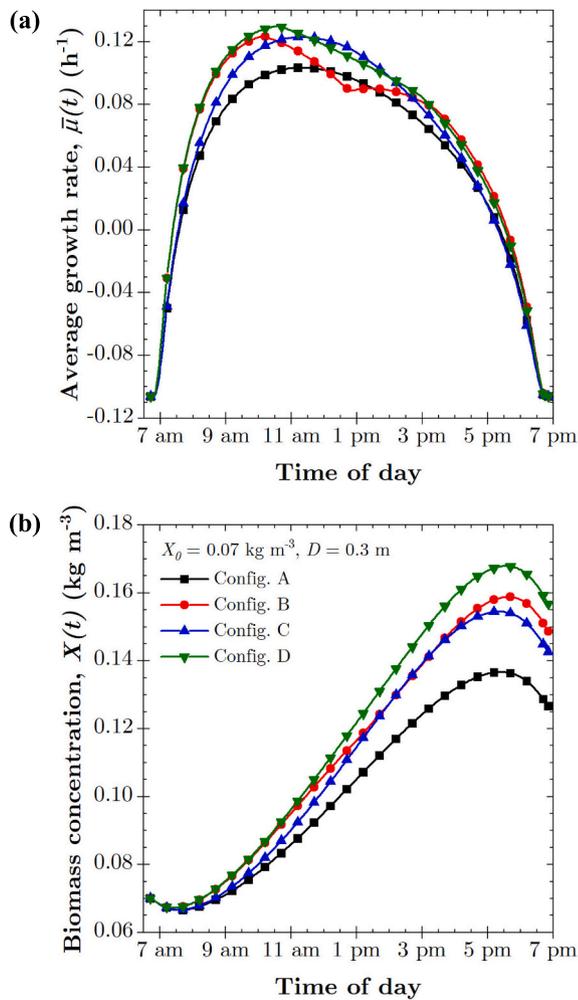
Fig. 5. (a) Average specific growth rate $\overline{\mu}(t)$ and (b) biomass concentration $X(t)$ as functions of time on September 21st for Configurations A–D located in Los Angeles, CA with initial biomass concentration $X_0 = 0.07 \, kg \, m^{-3}$ and culture depth $D = 0.3$ m.

C. vulgaris was used to predict the volume-averaged specific growth rate $\overline{\mu}(t)$ [Eqs. (12)–(13)]. Then, the biomass concentration at subsequent times $X(t + \Delta t)$ was predicted by integrating Eq. (11) and assuming that $\overline{\mu}(t)$ and $X(t)$ were constant over the time increment Δt according to

$$X(t + \Delta t) = X(t)[1 + \overline{\mu}(t)\Delta t] \qquad (17)$$

where the time increment Δt was equal to 3 min to obtain numerically converged results. This process was then repeated for the updated biomass concentration and sunlight parameters at $t = t + \Delta t$ until sunset, defined here as the time t where $\theta_z \geq 90°$.

3. Results and discussion

3.1. Incident radiative flux

Fig. 4a plots the fraction S_{ref}/S_C of the total culture area S_C receiving reflected light for Configurations A-D as a function of time on September 21st in Los Angeles, CA. Note that S_{ref}/S_C was zero throughout the day for Configuration A since no reflecting mirrors were present, i.e., $S_{ref} = 0$. Both Configurations B and D experienced a decrease in the reflected area S_{ref} at midday. This was due to the small apparent solar zenith angle $\theta_{z,a}$ at midday and the fact that the mirror height was limited to $H^*=1$ m (see Fig. 2b). The ratio of S_{ref}/S_C for Configuration B was nearly unity at the beginning and end of the day when the sun was positioned facing the

west and east mirror, respectively. On the other hand, $S_{ref}/S_C = 1$ for several hours in the morning and evening for Configuration D thanks to the tracking system which ensured that the sun was always facing the mirror. Note that a ratio S_{ref}/S_C equal to unity corresponds to a two-fold increase in the average incident flux $\overline{q}''_{in,PAR}$, the maximum achievable with a single planar mirror. Unlike Configurations B and D, the ratio S_{ref}/S_C for Configuration C was nearly zero in the morning and evening. At these times, the sun's rays were virtually parallel to the south-facing mirror and the reflected area S_{ref} was small. The ratio S_{ref}/S_C reached a maximum at midday for Configuration C but it never attained a value of unity, since the mirror height $H_C(t)$ was limited to H^* at midday when the sun was positioned facing the mirror (see Fig. 2b).

Fig. 4b plots the incident photosynthetic photon flux $\overline{q}''_{in,PAR}$ [Eq. (7)] averaged over the culture surface area as a function of time on September 21st for Configurations A–D. It indicates that Configurations B–D increased the mean incident photosynthetic photon flux throughout the day compared to a raceway pond without mirrors. In the morning and evening, Configurations B and D exhibited the highest mean incident photosynthetic flux thanks to the east- and west-facing orientation of their mirrors. Nonetheless, the incident photosynthetic flux remained small in the early morning and late evening due to the weak solar irradiation $G_{S,\lambda}$ at these times. Furthermore, the mean incident photosynthetic flux of Configuration B decreased at midday to be equal to that of Configuration A as the sun aligned with the north-south axis and the reflected area S_{ref} went to zero (see Fig. 4a). At midday, the mean incident photosynthetic flux was higher for Configuration C than Configuration B due to the south-facing orientation of the mirror.

3.2. Microalgae growth

Fig. 5a and 5b show the temporal evolution of the volume-averaged specific growth rate $\overline{\mu}(t)$ and the biomass concentration $X(t)$ on September 21st in Los Angeles, CA for the four raceway pond configurations considered. For all configurations, the initial biomass concentration was $X_0 = 0.07 \, kg \, m^{-3}$ and the culture depth was $D = 0.3$ m. Fig. 5a indicates that the average specific growth rate $\overline{\mu}(t)$ was higher for the raceway ponds featuring mirrors compared to Configuration A at nearly all times of day. This was thanks to the increased solar collection surface provided by the mirrors which increased the incident photosynthetic photon flux $\overline{q}''_{in,PAR}$, as observed in Fig. 4b. At midday, the effect of the mirrors in Configuration B was small and the average growth rate $\overline{\mu}(t)$ was briefly smaller than that of Configuration A. This was caused by the decrease in light penetration due to the higher biomass concentration $X(t)$ in Configuration B compared to Configuration A. In the morning and evening, Configuration B had a larger average growth rate $\overline{\mu}(t)$ than Configuration C, while the opposite was true at midday. This was attributed to the fact that the east/west facing mirrors increased the photosynthetic photon flux $\overline{q}''_{in,PAR}$ significantly in the mornings and evenings while the south-facing mirror increased $\overline{q}''_{in,PAR}$ the most at midday (see Fig. 4b). On the other hand, Configuration D had the highest average growth rate $\overline{\mu}(t)$ until 11 am thanks to its solar tracking capability. Throughout the rest of the day, the average growth rate $\overline{\mu}(t)$ of Configuration D decreased slightly compared to Configurations B and C due to the higher biomass concentration which reduced light penetration. In fact, $\overline{\mu}(t)$ was nearly the same for all four configurations at 6 pm due to the large biomass concentration and the low incident flux at the end of the day. These factors caused the illuminated volume of the culture to be very small, with or without mirrors present.

Similarly, Fig. 5b indicates that Configurations B–D yielded larger biomass concentration $X(t)$ than Configuration A at all times of the day on September 21st. Configuration D achieved the largest maximum biomass concentration of $X_{max} = 0.168 \, g \, L^{-1}$ compared to $X_{max} = 0.137 \, g \, L^{-1}$ for Configuration A. Configurations B and C reached a maximum biomass concentration X_{max} of 0.159 g L^{-1} and 0.155 g L^{-1}, respectively. For all configurations, X_{max} was attained around 5:30 pm.
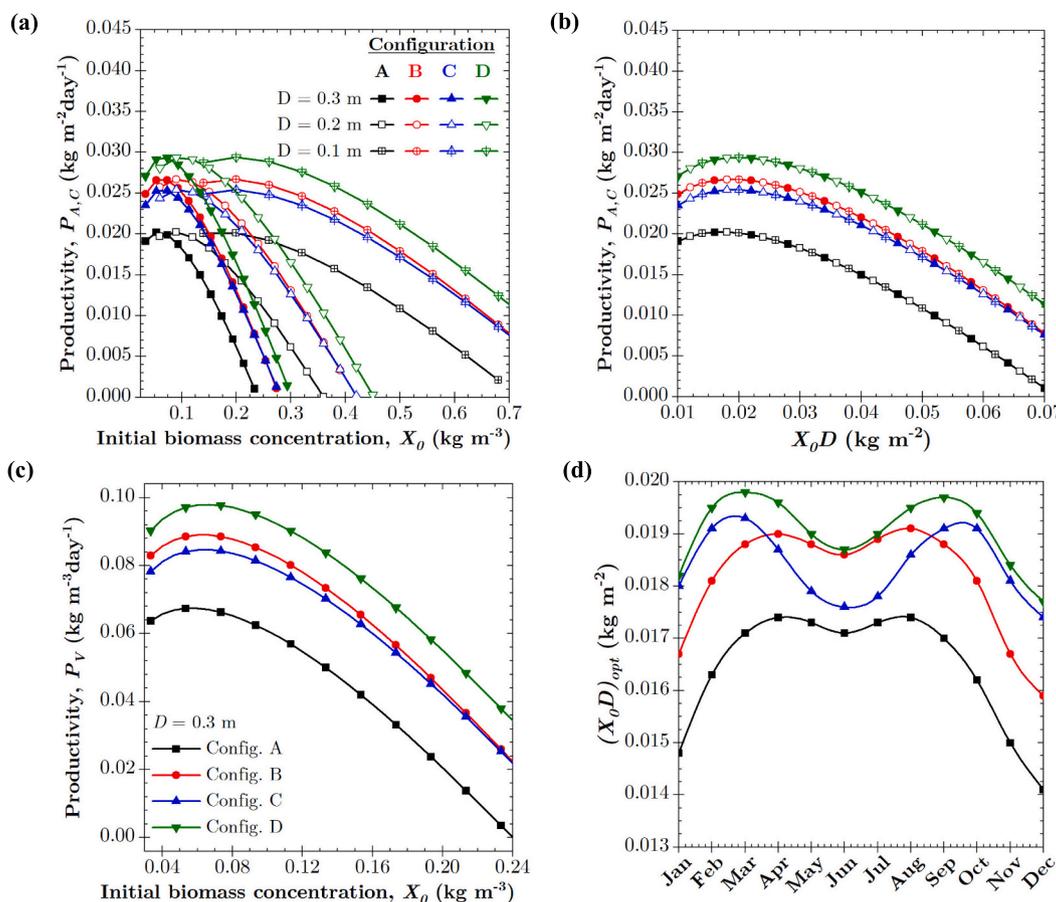
Fig. 6. Daily culture-area-based $P_{A,C}$ productivity as a function of (a) initial biomass concentration X_0 and (b) the product X_0D for culture depth D equal to 0.1 m, 0.2 m, and 0.3 m on September 21st. (c) Volumetric P_V productivity as function of X_0 for a culture depth $D = 0.3$ m on September 21st. (d) Product of the initial biomass concentration and the culture depth $(X_0D)_{opt}$ which maximizes biomass productivity on the 21st day of each month of the year. All data shown is for Configurations A–D located in Los Angeles, CA.

Interestingly, Configurations B and C exhibited similar growth curves despite marked differences in their designs (see Fig. 1B and 1C) and corresponding average incident photosynthetic photon flux $\overline{q}''_{in,PAR}$ (see Fig. 4b). Overall, the new reflecting pond designs increased the maximum biomass concentration X_{max} by 16%, 13%, and 23% for Configurations B, C, and D, respectively, compared to the traditional raceway pond of Configuration A. For all configurations, the biomass concentration $X(t)$ decreased after approximately 5:30 pm as the available photosynthetic photon flux was not sufficient to sustain growth resulting in biomass loss due to respiration.

3.3. Biomass productivity

Fig. 6a shows the daily culture-area-based $P_{A,C}$ biomass productivity of Configurations A-D as a function of the initial biomass concentration X_0 for culture depths D equal to 0.1 m, 0.2 m, and 0.3 m on September 21st in Los Angeles, CA. Previous studies [10,20] have demonstrated that the culture-area-based biomass productivity of photobioreactors and covered raceway ponds scales with X_0/a where a is the specific illuminated area given by $a = S_C/V$ such that $a = 1/D$ for the present raceway ponds. Note also that the initial culture optical thickness can be expressed as $\beta_{\lambda,0}D = (\overline{A}_{abs,\lambda} + \overline{S}_{sca,\lambda})X_0D$ where $\beta_{\lambda,0}$ is the initial extinction coefficient in m^{-1}. Thus, the product X_0D of the initial biomass concentration X_0 and the culture thickness D is representative of the culture's initial optical thickness [10]. Fig. 6b plots the same data for biomass productivity $P_{A,C}$ shown in Fig. 6a but as a function of X_0D. The results indicate that, even when using mirrors, the productivity $P_{A,C}$

collapsed onto a single line for all values of X_0 and D. Note that land-area-based biomass productivity $P_{A,L} = P_{A,C} \times S_C/S_L$ (not pictured) also collapsed onto a single line. This indicates that the scaling relation between areal biomass productivity (in kg m^{-2} day^{-1}) and the initial optical thickness represented by the product X_0D holds true for raceway ponds featuring external mirrors.

Fig. 6c shows the daily volumetric biomass productivity P_V for all four raceway pond configurations as a function of X_0 for a culture depth $D = 0.3$ m on September 21st in Los Angeles, CA. Note that volumetric productivity is given by $P_V = P_{A,C}/D$ and thus did not scale with the product X_0D. Configurations B–D significantly improved the daily culture-area-based $P_{A,C}$ and volumetric P_V biomass productivities for all values of X_0D and X_0, respectively. The maximum value of both $P_{A,C}$ and P_V increased by 32%, 26%, and 45% for Configurations B, C, and D, respectively, compared to Configuration A for which $P_{A,C,max} = 0.020$ kg m^{-2} day^{-1} and $P_{V,max} = 0.067$ kg m^{-3} day^{-1}. The predicted productivity of Configuration A was within the typical range of productivities for well-managed open raceway ponds reported as 0.020 to 0.025 kg m^{-2} day^{-1} from Ref. [5].

Fig. 6d plots the optimum value of the product X_0D which yielded the maximum biomass productivity on the 21st day of each month of the year, denoted by $(X_0D)_{opt}$, for Configurations A–D in Los Angeles, CA. The smallest optimum initial optical thickness represented by $(X_0D)_{opt}$ occurred during the winter months for all four configurations. During this time of year, the optimum optical thickness was lower due to the decreased incident photon flux. Similarly, $(X_0D)_{opt}$ of Configuration A was smaller than that of Configurations B–D throughout the year due to its lower incident photon flux. However, all four configurations

(a)

(b)
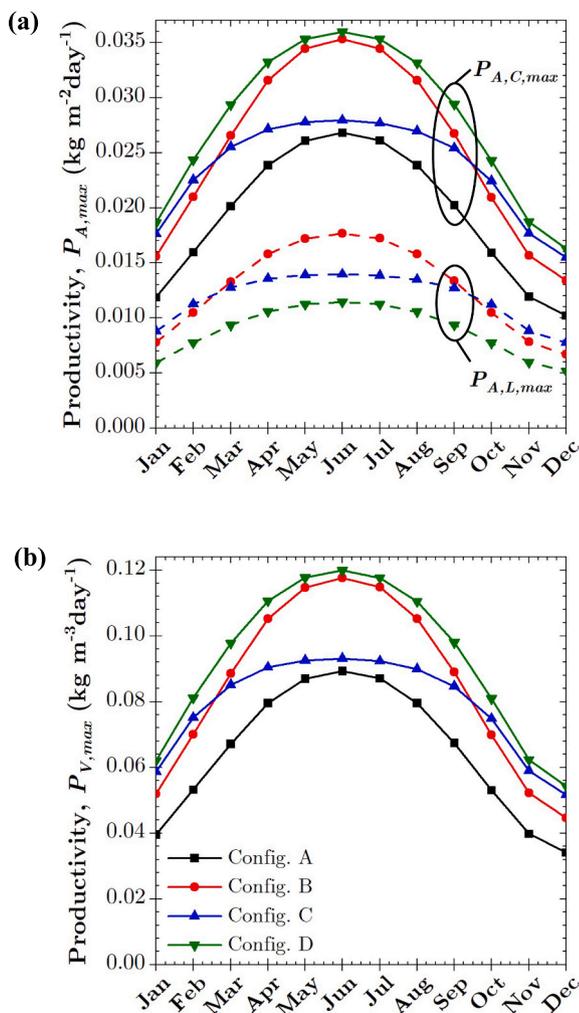
Fig. 7. (a) Maximum daily culture-area-based $P_{A,C,max}$, land-area-based $P_{A,L,max}$, and (b) volumetric $P_{V,max}$ productivity over one year for raceway pond Configurations A–D in Los Angeles, CA.

(a)

(b)

Fig. 8. Maximum daily culture-area-based biomass productivity $P_{A,C,max}$ as a function of normalized maximum mirror height H^*/W on September 21st for Configurations A–D in (a) Los Angeles, CA and (b) Saint-Nazaire, France.

exhibited a local minimum in $(X_0D)_{opt}$ during June when the incident photon flux was the largest. This was attributed to the longer days during the summer months which led to higher biomass concentrations in the afternoon. Thus, $(X_0D)_{opt}$ was smaller to avoid low light penetration and small growth rates in the afternoon. The maximum in $(X_0D)_{opt}$ occurred in April and August for Configurations A and B and in March and September for Configurations C and D. These results suggest that both the solar intensity and duration of the day must be considered to identify $(X_0D)_{opt}$ for a given location and time of year.

Fig. 7a and b shows the maximum daily culture-area-based $P_{A,C,max}$, land-area-based $P_{A,L,max}$, and volumetric $P_{V,max}$ productivities of Configurations A-D obtained from simulations of biomass concentration $X(t)$ from sunrise to sunset on the 21st day of each month of the year using $(X_0D)_{opt}$ reported in Fig. 6d. It is evident that adding mirrors to the raceway pond increased the maximum biomass productivities $P_{A,C,max}$ and $P_{V,max}$ throughout the year. Indeed, even the simple single-mirror design of Configuration C increased the culture-area-based $P_{A,C,max}$ and volumetric $P_{V,max}$ productivities by 52% in December. However, Configurations B–C also decreased the maximum land-area-based $P_{A,L,max}$ productivity throughout the year. Configuration D exhibited the largest culture-area-based $P_{A,C,max}$ and volumetric $P_{V,max}$ productivities as well as the smallest land-area-based $P_{A,L,max}$ productivity. This was due to the additional land area required to accommodate the rotating platform and prevent shading between adjacent ponds with external mirrors. Thus, a production facility featuring raceway ponds of

Configuration D would require a larger land area to achieve the same annual yield as a raceway pond of Configuration A–C. Furthermore, Fig. 7 indicates that Configuration B had larger productivities $P_{A,C,max}$, $P_{A,L,max}$, and $P_{V,max}$ from March to September than Configuration C while the opposite was true from October to February. This suggests that the dual mirror design of Configuration B is better suited to smaller solar zenith angles θ_z observed in the summer months. Conversely, the single mirror design of Configuration C is better suited to larger solar zenith angles θ_z observed in the winter months.

3.4. Impact of reflecting pond dimensions and location

The maximum daily culture-area-based biomass productivity $P_{A,C,max}$ was predicted for pond length-to-width ratio L/W ranging from 1 to 20 for Configurations A–D in Los Angeles, CA on September 21st. The results are shown in Fig. S2 of Supplementary Materials. The productivity $P_{A,C,max}$ of Configuration A was found to be independent of L/W as light transfer within the culture was modeled as one-dimensional and ignored edge effects. This was also the case for Configuration D thanks to its tracking feature which ensured that no reflected light fell outside of the culture surface (see Fig. 1D). On the other hand, the biomass productivity $P_{A,C,max}$ of Configurations B and C increased as the length-to-width ratio L/W increased up to $L/W \sim 5$, beyond which a plateau was reached. This was due to a decrease in the fraction of total reflected light that fell outside of the culture surface (see Fig. 1B and 1C) as L/W increased. Thus, raceway ponds featuring mirrors should have a length-
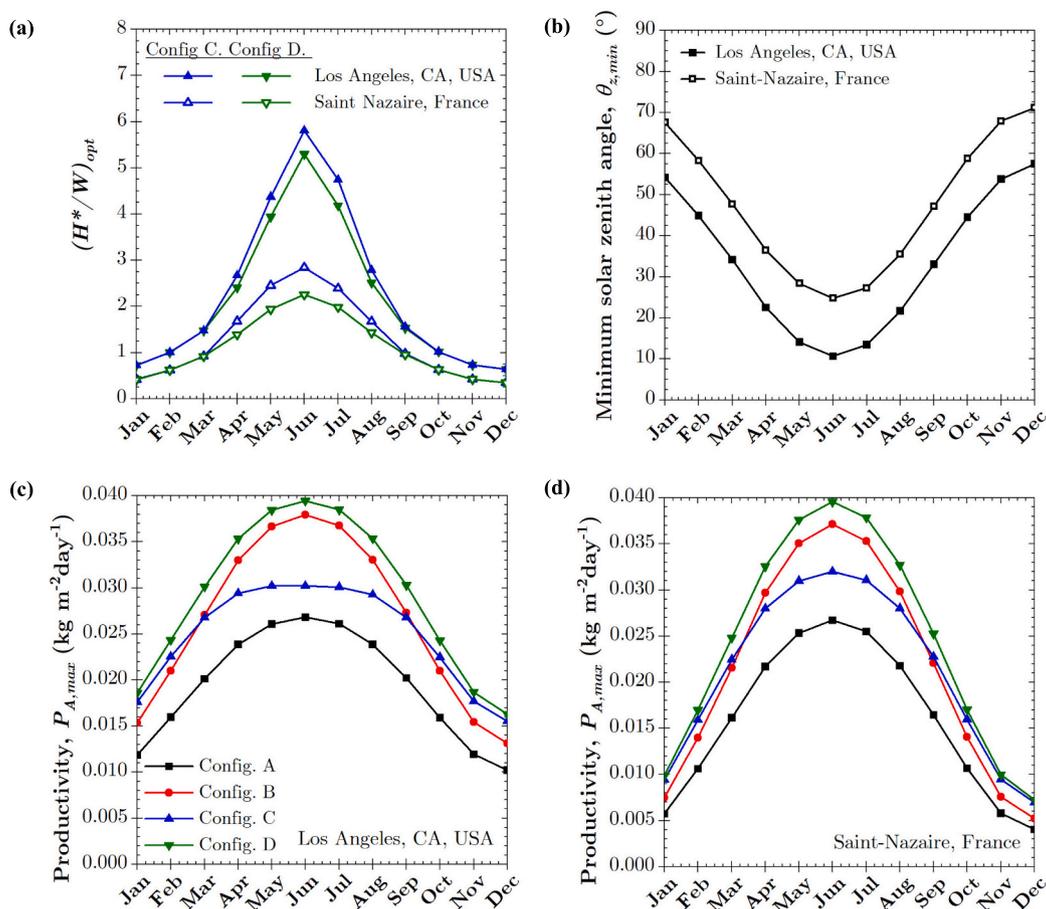
Fig. 9. (a) Optimum mirror height normalized by the pond width $(H^*/W)_{opt}$ for Configurations C and D and (b) the minimum solar zenith angle $\theta_{z,min}$ on the 21st day of each month in Los Angeles, CA and Saint-Nazaire, France. Maximum daily culture-area-based biomass productivity $P_{A,C,max}$ throughout the year using $(H^*/W)_{opt}$ for Configurations A–D located in (c) Los Angeles, CA and (d) Saint-Nazaire, France.

to-width ratio $L/W \geq 5$ to mitigate this effect. The impact of L/W was found to be the same throughout the year (see also Supplementary Materials).

Fig. 8a and 8b plots the maximum daily culture-area-based biomass productivity $P_{A,C,max}$ as a function of the maximum allowed mirror height normalized with respect to the pond width H^*/W for Configurations A–D on September 21st in Los Angeles, CA and Saint-Nazaire, France. For the dual east/west mirror Configuration B, Fig. 8 indicates that the productivity $P_{A,C,max}$ increased continuously with increasing H^*/W for both locations. This was due to the fact that the apparent solar zenith angle $\theta_{z,a}$ approached zero at midday which resulted in very large values of mirror height required to maximize the reflected area according to Eq. (2). On the other hand, the productivity $P_{A,C,max}$ of Configurations C and D increased and then remained constant for $H^*/W \geq 1.6$ for Los Angeles, CA and $H^*/W \geq 1.0$ for Saint-Nazaire, France. Thus, these values represented the optimum value $(H^*/W)_{opt}$ of the maximum mirror height H^* normalized by the pond width W. Note that $(H^*/W)_{opt}$ for Configurations C and D on September 21st were given by the maximum value of mirror height $H_{C/D}(t)$ on that day from Eqs. (3) and (4), respectively. Thus, the mirror height required to optimize the productivity of a raceway pond can be readily calculated for any given configuration, location, and day of the year.

Fig. 9a plots the optimum mirror height normalized by the pond width $(H^*/W)_{opt}$ for the 21st day of each month in Los Angeles, CA and Saint-Nazaire, France for Configurations C and D. Note that $(H^*/W)_{opt}$ was not shown for Configuration B since it was infinite at midday as the apparent solar zenith angle $\theta_{z,a}$ approached zero [see Eq. (2)]. Fig. 9a indicates that $(H^*/W)_{opt}$ was smaller throughout the year at the higher

latitude of Saint-Nazaire, France compared to that of Los Angeles, CA. This was due to the larger minimum solar zenith angle $\theta_{z,min}$ (see Fig. 9b) which reduced the mirror height necessary to maximize the fraction S_{ref}/S_C of the culture area subjected to reflected light. Similarly, the larger solar zenith angles in the winter months resulted in smaller $(H^*/W)_{opt}$ compared to the summer months for both locations. Furthermore, Fig. 9a demonstrates that the mirror heights required to optimize the performance of both configurations were small in the winter months, particularly for ponds located in Saint-Nazaire where $(H^*/W)_{opt}$ was less than unity from September to March.

Fig. 9c and 9d plot the predicted maximum culture-area-based productivity $P_{A,C,max}$ throughout the year for the optimum maximum mirror height $(H^*/W)_{opt}$ from Fig. 9a for all four configurations in Los Angeles, CA and Saint-Nazaire, France, respectively. Here, the optimum maximum mirror height $(H^*/W)_{opt}$ for Configuration C was used for Configuration B. In general, Fig. 9c and 9d indicate that the areal productivity $P_{A,C,max}$ for raceway ponds located in Los Angeles was greater than those located in Saint-Nazaire. This can be attributed in part to the smaller solar zenith angles (see Fig. 9b) experienced by the ponds in Los Angeles thanks to its lower latitude. However, Configuration C yielded a slightly larger productivity in Saint-Nazaire than in Los Angeles during the month of June despite having a significantly smaller optimum mirror height H^* (see Fig. 9a) and experiencing a larger solar zenith angle θ_z. This indicates that Configuration C was more effective at improving the biomass productivity of raceway ponds at higher latitudes. Furthermore, for Saint-Nazaire, the productivity of Configuration C was nearly equal to the ideal tracking case of Configuration D from October to February. Indeed, volumetric and culture-area-based productivity increased by up

to 73% for Configuration C in Saint-Nazaire during these months despite the relatively small optimum maximum mirror height ($H^*/W)_{opt}$.

Overall, Configurations B–D enabled higher biomass yield per unit area and volume of culture by increasing the solar input to the micro-algae culture. This would reduce the final cost per unit mass of biomass since the operating cost scales linearly with the culture surface area [18]. Moreover, by increasing productivity in the winter months, the growing season can be extended and yearly productivity can be improved in locations where year-long growth is currently inefficient. For example, Configuration C increased biomass production in Saint-Nazaire from September to March by 50%. Additionally, the increased incident solar flux achieved by using mirrors may decrease the energy required for thermal regulation of the culture in cooler months and/or climates where sunlight is a major source of heat for solar culture systems [21]. However, adding mirrors requires more land to prevent mutual shading between adjacent raceway ponds. Furthermore, the mirrors and control system required to implement the external reflecting pond design would increase the capital and maintenance costs compared to a standard raceway pond, particularly for Configuration B featuring two mirrors and for Configuration D featuring the rotating raceway pond. Thus, Configuration C appears to be the most practical design as it requires a single mirror but still improved the raceway pond volumetric and culture-area-based biomass productivity significantly, particularity in the winter months. The concepts explored in this study are promising and should be explored experimentally.

4. Conclusion

The use of mirrors to increase the daily biomass productivity of outdoor raceway ponds by reflecting additional light onto the micro-algae culture was investigated theoretically. Four designs were considered including a raceway pond without mirrors (Configuration A) used as a reference, a pond oriented along the north/south axis with mirrors on both its east and west sides (Configuration B), a pond oriented along the east/west axis with a single mirror on its north side (Configuration C), and a solar tracking rotating pond with a single mirror (Configuration D). The growth of *Chlorella vulgaris* was predicted using the two-flux approximation and a growth kinetics model accounting for light limitation and cell respiration activity. The use of external mirrors was found to improve the daily volumetric and culture-area-based biomass productivities throughout the year and by as much as 73% compared to a raceway pond without mirrors. Configuration B outperformed Configuration C in the summer months, while the opposite was true in the winter months. Furthermore, the culture-area-based biomass productivity of all four configurations was found to scale by the product of the initial biomass concentration and the culture depth X_0D. The product X_0D which yielded the maximum biomass productivity depended on the configuration and the time of year. The addition of mirrors was found to yield the largest improvement in biomass productivity for ponds with a pond length-to-width ratio greater than 5. Additionally, the optimum maximum mirror height was reported for Configurations C and D for both Los Angeles, CA, and Saint-Nazaire, France. Overall, Configuration C featuring a single mirror on the north side of a pond oriented along the east-west axis was considered to be the simplest and most cost-effective method for improving the biomass productivity in outdoor raceway ponds. These results provide practical guidelines for the design and operation of raceway ponds featuring mirrors for improved biomass productivity.

CRediT authorship contribution statement

Jack Hoeniges: Conceptualization, Methodology, Software, Validation, Investigation, Writing – original draft, Writing – review & editing, Visualization. **William Welch:** Software, Validation, Resources, Writing – review & editing. **Jeremy Pruvost:** Conceptualization, Software, Writing – review & editing, Supervision, Funding acquisition.

Laurent Pilon: Conceptualization, Writing – review & editing, Supervision, Funding acquisition.

Declaration of competing interest

The authors declare that they have no known competing financial interests or personal relationships that could have appeared to influence the work reported in this paper.

Acknowledgment

Appendix A. Supplementary material

Supplementary material to this article can be found online at https://doi.org/10.1016/j.algal.2022.102742.

References

[1] Y. Chisti, Biodiesel from microalgae, Biotechnol. Adv. 25 (3) (2007) 294–306.
[2] J. Matos, C. Cardoso, N.M. Bandarra, C. Afonso, Microalgae as healthy ingredients for functional food: a review, Food Funct. 8 (8) (2017) 2672–2685.
[3] D. Jha, V. Jain, B. Sharma, A. Kant, V.K. Garlapati, Microalgae-based pharmaceuticals and nutraceuticals: an emerging field with immense market potential, ChemBioEng Rev. 4 (4) (2017) 257–272.
[4] J. Pruvost, J.-F. Cornet, L. Pilon, Large-scale production of algal biomass: photobioreactors, in: F. Bux, Y. Chisti (Eds.), Algae Biotechnology: Products and Processes, Springer International Publishing, Switzerland, 2016, pp. 41–66.
[5] M.R. Tredici, Mass production of microalgae: photobioreactors, in: A. Richmond (Ed.), Handbook of Microalgal Culture: Biotechnology and Applied Phycology, Blackwell Publishing Ltd, Cornwall, UK, 2004, pp. 178–214, chapter 9.
[6] M.F. Modest, Radiative Heat Transfer, 3rd edition, Elsevier Inc, Oxford, UK, 2013.
[7] J. Pruvost, J.-F. Cornet, V. Goetz, J. Legrand, Theoretical investigation of biomass productivities achievable in solar rectangular photobioreactors for the cyanobacterium Arthrospira platensis, Biotechnol. Prog. 28 (3) (2012) 699–714.
[8] A. Souliès, J. Legrand, H. Marec, J. Pruvost, C. Castelain, T. Burghelea, J.-F. Cornet, Investigation and modeling of the effects of light spectrum and incident angle on the growth of Chlorella vulgaris in photobioreactors, Biotechnol. Prog. 32 (2) (2016) 247–261.
[9] J. Pruvost, J.-F. Cornet, F. Le Borgne, V. Goetz, J. Legrand, Theoretical investigation of microalgae culture in the light changing conditions of solar photobioreactor production and comparison with cyanobacteria, Algal Res. 10 (2015) 87–99.
[10] E. Lee, J. Pruvost, X. He, R. Munipalli, L. Pilon, Design tool and guidelines for outdoor photobioreactors, Chem. Eng. Sci. 106 (2014) 18–29.
[11] J.-F. Cornet, C.G. Dussap, G. Dubertret, A structured model for simulation of cultures of the cyanobacterium Spirulina platensis in photobioreactors: I. Coupling between light transfer and growth kinetics, Biotechnol. Bioeng. 40 (7) (1992) 817–825.
[12] J.-F. Cornet, C.G. Dussap, J.B. Gros, C. Binois, C. Lasseur, A simplified monodimensional approach for modeling coupling between radiant light transfer and growth kinetics in photobioreactors, Chem. Eng. Sci. 50 (9) (1995) 1489–1500.
[13] L. Pottier, J. Pruvost, J. Deremetz, J.-F. Cornet, J. Legrand, C.-G. Dussap, A fully predictive model for one-dimensional light attenuation by Chlamydomonas reinhardtii in a torus photobioreactor, Biotechnol. Bioeng. 91 (5) (2005) 569–582.
[14] J. Pruvost, J.-F. Cornet, Knowledge models for the engineering and optimization of photobioreactors, in: C. Posten, W. Christian (Eds.), Microalgal Biotechnology: Potential and Production, De Gruyter, Berlin, DE, 2012, pp. 181–224, chapter 10.
[15] I. Dunn, E. Heinzle, J. Ingham, J. Prenosil, Biological Reaction Engineering: Dynamic Modelling Fundamentals With Simulation Examples, 2nd edition, Wiley-VCH, Weinheim, Germany, 2003.
[16] H. Takache, J. Pruvost, J.-F. Cornet, Kinetic modeling of the photosynthetic growth of Chlamydomonas reinhardtii in a photobioreactor, Biotechnol. Prog. 28 (2012) 681–692.
[17] J. Pruvost, Cultivation of algae in photobioreactors for biodiesel production, in: A. Pandey, C. Larroche, C.G. Dussap, E. Gnansounou, S.K. Khanal, S. Ricke (Eds.), Biofuels: Alternative Feedstocks and Conversion Processes for the Production of Liquid and Gaseous Biofuels, 2 edition, Academic Press, San Diego, CA, 2019, pp. 629–659, chapter 26.

[18] I. Gifuni, A. Pollio, C. Safi, A. Marzocchella, G. Olivieri, Current bottlenecks and challenges of the microalgal biorefinery, Trends Biotechnol. 37 (3) (2019) 242–252.

[19] C. Gueymard, Simple model of the atmospheric radiative transfer of sunshine (SMARTS). http://rredc.nrel.gov/solar/models/SMARTS, 2005. Version 2.9.5.

[20] J. Hoeniges, K. Zhu, J. Pruvost, J. Legrand, E.-K. Si-Ahmed, L. Pilon, Impact of dropwise condensation on the biomass production rate in covered raceway ponds, Energies 14 (2) (2021) 1–24.

[21] J. Pruvost, V. Goetz, A. Artu, P. Das, H.Al Jabri, Thermal modeling and optimization of microalgal biomass production in the harsh desert conditions of State of Qatar, Algal Res. 38 (101381) (2019).